Invited MML'95, Cambridge, JMMM

Magneto-Optical and Photoemission Studies of Ultrathin Wedges*

S.D. Bader and Dongqi Li

Materials Science Division
Argonne National Laboratory, Argonne, IL 60439

***INVITED:** 2nd International Symposium on Metallic Multilayers (MML'95), September 11-14, 1995, Cambridge, UK, to be published in Jour. Magn. Magn. Mater.*

*Work supported by the U.S. Department of Energy, Basic Energy Sciences-Materials Sciences, under contract #W-31-109-ENG-38.

Magneto-optical and Photoemission Studies of Ultrathin Wedges*

S. D. Bader and Dongqi Li

Materials Science Division, Argonne National Laboratory, Argonne, IL 60439

Magnetic phase transitions of Fe wedges grown epitaxially on Cu(100) are detected via the surface magneto-optical Kerr effect and used to construct a phase diagram for face centered Fe. Also, the confinement of Cu *sp*- and *d*-quantum-well states is studied for Cu/Co(wedge)/Cu(100) utilizing undulator-based photoemission experiments.

Keywords: fcc Fe; phase diagram; quantum well states

Corresponding author: S. D. Bader

I. Introduction

Surface and thin-film magnetism represents a rapidly developing area of materials research due to the observation of new phases and new effects in ultrathin layered structures. Examples of present interest include the exploration of face-centered phases of Fe, and the oscillatory interlayer magnetic coupling and giant magnetoresistence (GMR) of magnetic heterostructures. The ability to make atomically flat layers with sharp interfaces and continuous thickness variations permits new insights to be gained into relationships between structural, electronic and magnetic properties. Herein we review highlights of two wedge studies that pertain to epitaxial Fe/Cu(100) and Cu/Co/Cu(100) film systems. The first is a surface magneto-optical Kerr effect (SMOKE) study of epitaxial-stabilized, face-centered phases of Fe grown on Cu(100). We present a phase diagram and focus on the fcc antiferromagnetic (AF) phase that possesses a ferromagnetic (F) surface layer. The second is a photoemission study of Cu/Co(wedge)/Cu(100), in which the confinement of *sp*- and *d*-quantum-well (QW) states of a two-monolayer (ML) Cu overlayer are characterized and related to the GMR properties of related Co/Cu multilayers.

II. Experiment

Sample preparation and characterization[1,2] and background for SMOKE[3] and spin-polarized photoemission[4] experments have been reported elsewhere. The Cu(100) substrates were cleaned in ultrahigh vacuum (UHV) via standard sputtering and annealing cycles. Wedge-shaped samples with slopes of ~2-3 Å/mm were fabricated *in-situ* via UHV-evaporation by moving the substrate behind a mask during growth. Deposition rates were typically 0.4-1 Å/min. All films grew epitaxially in face centered phases with (100) orientation, as indicated by low- and reflection high-energy electron diffraction (LEED and RHEED), except for the thick Fe on Cu(100) that transformed to the equilibrium bcc phase. SMOKE measurements utilized a He-Ne laser that was focused to ~0.2 mm diameter and scanned along the wedge. Hysteresis loops were generated by measuring the Kerr

ellipticity *vs.* applied magnetic field. The remanent magnetization M_R for the different phases is reported in arbitrary units. Angle- and/or spin-resolved photoemission spectra utilized the U5 undulator beamline at the National Synchrotron Light Source. The spot size was ~1 mm, and spectra were taken at normal emission with a photon energy of 22.7 eV and resolution of 0.15-0.20 eV.

III. Results

A. Fe/Cu(100)

Fe/Cu(100) is a rich and controversial magnetic system with several phases. Complications arise from the intrinsic magnetic instabilities of fcc Fe, and the structural instabilities that are influenced by growth conditions, such as changes in substrate temperature T_S, as illustrated in Fig. 1.[1] All films transform to bcc in the thick limit of ~10-12 ML Fe. Below that threshold, the thickness dependence of M_R is qualitatively different for wedges grown at different temperatures. For low-T_S values (with the sample subsequently annealed to room temperature) there is a spin-reorientation transition at ~ 6 ML of Fe, in which the magnetic easy axis changes from perpendicular to in-plane with increasing Fe thickness, while the structure remains intact in a tetragonally-distorted fcc phase (fct). Pappas *et al.*[5] first showed that this transition is reversible on temperature cycling. The transition originates from a competition between the surface magnetic and shape anisotropies, and has attracted much theoretical attention recently.[6]

For films grown near room temperature (RT), the phase transition at ~ 5-ML Fe is qualitatively different from that for low-T_S growth. The Fe is F between 2-5 ML with a perpendicular easy axis, as before, but it is AF between ~ 6-11 ML with a F-surface layer that is perpendicularly aligned (see Fig. 1). EXAFS results[7] suggest that the first phase is fct, as mentioned above, while the second phase is relatively undistorted fcc-like. These phases typically show different reconstruction patterns in LEED: 4x1 or 5x1 for fct, and 1x1 or 2x1 for fcc. The bcc phase of the thicker films typically shows a more complicated

"3x1"-based pattern.[8] Recent structural studies report that the fct phase has a periodic distortion[9] and the fcc phase a sheer transformation and a rotation with respect to the substrate.[10] A Mössbauer study reported the coexistence of high-spin F and low-spin AF phases while dilating the lattice parameter via alloying for Cu-Au(100) substrates.[11]

Of particular interest is the phase for 6-11 ML of Fe grown at RT. The M_R value is much smaller than that of the 4-ML Fe thickness. Instead of linearly increasing with film thickness, the M_R maintains a constant plateau at elevated temperature and shows a two-peaked structure at lower T. The signal is sensitive to the background pressure during growth, which suggests that it originates from a F-surface phase.[1,12] This hypothesis is plausible because of the known outward surface relaxation and resultant large volume/atom in the surface layer that would favor ferromagnetism.[13] We interpret the magnetic response as rising from an AF phase that consists of F layers in an antiparallel stacking sequence with an enhanced F surface signal. We take the peak-to-valley difference of the M_R (ΔM_R) as an indication of incomplete compensation within the AF stack, and the average M_R value as the indicator of the surface F phase. The temperature dependence of the interior and surface magnetic signals are shown in Fig. 2. The M_R data indicate a surface T_C value of 250 K. The ΔM_R data are initially linear and extrapolate to zero to define a Néel temperature of $T_N \sim 200$ K. The value of T_N is much higher than the ~ 67 K reported for both Fe precipitates in a Cu host and for Fe films. But the high value disappears when the surface magnetism is destroyed by contamination. This suggests that the AF signal may be bootstrapped by the surface magnetism, via either proximity or a spin density wave (SDW) formation. Our results are supported by a recent theoretical calculation,[14] where for 4-11 ML of Fe on Cu(100), the surface and subsurface layers are F-coupled while deeper layers are AF-coupled, and the intralayer couplings are always ferromagnetic.

The magnetic phase diagram of Fe/Cu(100) in Fig. 3 is plotted as growth temperature *vs.* Fe thickness. At low T_S the initial phase is ferromagnetic with a spin-

reorientation transition. For growth at RT the initial phase is ferromagnetic in the range of 2-5 ML, and from 6-11 ML the novelty is in the AF phase with a F surface layer. Finally, the films convert to the stable bcc phase at the thick limit.

B. Cu/Co/Cu(100)

Ortega and coworkers[15] established that the oscillatory interlayer magnetic coupling of ferromagnetic layers through nonmagnetic spacer layers correlates with the existence of spin-polarized QW states in the spacer that sweep through the Fermi level E_F as a function of spacer thickness. Although QW states in ultrathin metallic films had been discovered earlier, the correlation stimulated extensive new electron-spectroscopic investigations.[2,15-19] As shown in Fig. 4, the QW states shift in binding energy with Cu thickness for Cu overlayers deposited on thick Co(100) [that is grown on Cu(100)]. The QW states are due to finite-size effects, where the electron wavefunctions reflect from each interface/surface and interfere constructively or destructively. The quantization condition for the formation of these states is $2kd+\Phi_A+\Phi_B=2n\pi$, where k is the wavevector, Φ_A and Φ_B are phase shifts at the solid-vacuum and solid-solid interfaces, and n is an integer.[20-22] The phase shifts are determined by the relative heights of the energy potentials of the adjacent media. In addition to the well-studied *sp*-QW states at 0-3 eV binding energies, we also identify *d*-QW states at ~ 3 eV, as marked in Fig. 4. The *d*-states are discrete at least for 1-3 ML of Cu. The inset of Fig. 1 shows the Cu bulk bands that give rise to the QW states. The *sp*-QW states are derived from the Δ_1 band and the *d*-QW states from the Δ_5 band. The *d*-band quantization ought to be particularly important for magnetic coupling across transition-metal spacers, where the *d*-bands are at E_F. Both the *sp*-QW states and the *d*-states are spin polarized with minority character.[2] The minority spin electrons experience a deeper potential well than the majority electrons. Due to the exchange splitting in Co the majority band is close in energy to those of Cu. The spin-polarization of the QW states is important since it supports a SDW in the spacer perpendicular to the surface. The SDW mediates the

coupling of the magnetic layers. The period for the QW states to cross E_F and for the oscillatory coupling are the same and are determined by Fermi surface calipers.[15,23] The QW states of interest to the coupling problem are established for the F configuration of the multilayer structure, but each time a new QW state emerges at E_F the system becomes unstable and reverts to an AF configuration.[24] In the vacuum/spacer/F structures we study, the vacuum interface provides a barrier similar to an F layer.

The degree of confinement of QW states varies with the barrier height and width, *i.e.* the potential and the thickness of the ferromagnetic layer.[2] Figure 5 shows how the QW states of 2 ML of Cu at 1.6 (*sp*-) and 2.4 eV (*d*-state) evolve with Co thickness along a Co wedge that separates the Cu overlayer from the Cu(100) substrate. The intensity changes are plotted in Fig. 6. The *sp*-QW state is more weakly confined than the *d*-state. The *sp*-state intensity saturates at a thicker Co barrier than the *d*-state, where the characteristic barrier thicknesses are 2.2±0.6 and 0.6±0.2 Å, respectively. This is consistent with a deeper well and larger effective mass of the *d*-electrons as estimated via tight-binding calculations.[2]

The existence of a minimum barrier thickness to form QW states correlates with magnetic properties of interest in multilayers. Parkin[25] showed that a thin Co layer at the interface of a Cu/permalloy multilayer enhances the GMR exponentially with a characteristic thickness scale of 2.3 Å. As shown in Fig. 6, a Co layer of similar thickness is sufficient to establish the spin-polarized QW states in a Cu layer confined by the Co potentials. This in turn determines the strength of the interlayer coupling. Since the GMR accompanies the AF-coupling and occurs when an applied magnetic field forces the magnetization of different layers into parallel alignment, the evolution of the QW states should also impact the GMR behavior.

QW states have now been correlated with additional magnetic properties. It was shown recently that for Au/Fe/Au[26] and Au/Co/Au[27] the magneto-optical response oscillates with Fe or Au thickness, which was explained in terms of QW states in the films.

Carl and Weller[28] showed that the high-field paramagnetic magneto-optical response of Ru on Co can also oscillate with thickness, as attributed to Ru QW states. Johnson *et al.*[18] showed that the in-plane effective mass of the Cu QW states are enhanced below 8 ML of Cu due to interfacial hybridization. Since this should change the "dog bone" Fermi surface away from the zone center, the oscillation periods based on these extremal orbits should disappear. This explains why the short-period oscillations in Co/Cu/Co have only been observed for thick Cu layers.[29]

IV. Conclusions

Magnetic properties investigations of novel wedge systems have been highlighted, including SMOKE studies to construct a new phase diagram for Fe/Cu(100), and photoemission studies to examine quantum confinement of overlayer states in Cu(2 ML)/Co(wedge)/Cu(100). The former study identified a novel AF phase of fcc Fe with a F surface layer. The latter study provides insights into the origin of the oscillatory interlayer magnetic coupling and GMR of metallic multilayers.

* Work supported by the U.S. DOE BES-MS under contract W-31-109-ENG-38, and by the ONR under contract N-00014-94-F-0085.

REFERENCES

1. Dongqi Li, M. Freitag, J. Pearson, Z. Q. Qiu and S. D. Bader, Phys. Rev. Lett. **72**, 3112 (1994).
2. Dongqi Li, J. Pearson, P. D. Johnson, J. E. Mattson and S. D. Bader, Phys. Rev. B **51**, 7195(1995).
3. S. D. Bader, J. Magn. Magn. Mater. **100**, 440-454 (1991).
4. P. D. Johnson *et al.*, Rev. Sci. Inst. **63**, 1902 (1992).
5. D. P. Pappas, K.-P. Kämper and H. Hopster, Phys. Rev. Lett. **64**, 3179 (1990); D. P. Pappas, K. P. Kamper, B. P. Miller, H. Hopster, D. E. Fowler, A. C. Luntz, C. R. Brundle and Z. X. Shen, J. Appl. Phys. **69**, 5209-5211 (1991).
6. See references in S. D. Bader, Dongqi Li and Z. Q. Qiu, J. Appl. Phys. **76**, 6419 (1994).
7. H. Magnon *et al.*, Phys. Rev. Lett. **67**, 859 (1991).
8. F. Scheurer, R. Allenspach, P. Xhonneux, and E. Courtens, Phys. Rev. B **48**, 9890 (1993).
9. S. Müller, P. Bayer, C. Reischl, K. Heinz, B. Feldmann, H. Zillgen, and M. Wuttig, Phys. Rev. Lett. **74**, 765 (1995).
10. J. V. Barth and D. E. Fowler, unpublished preprint.
11. D. J. Keavney, D. F. Storm, J. W. Freeland, I. L. Grigorov and J. C. Walker, Phys. Rev. Lett. **74**, 4531 (1995).
12. J. Thomasen, F. May, B. Feldmann, M. Wuttig, and H. Ibach, Phys. Rev. Lett. **69**, 3831 (1992).
13. C. S. Wang, B. M. Klein and H. Krakauer, Phys. Rev. Lett. **54**, 1852 (1985); V. L. Moruzzi, P. M. Marcus, K. Schwarz and P. Mohn, Phys. Rev. B 34, 1784 (1986).
14. T. Kraft, P. M. Marcus and M. Scheffler, Phys. Rev. B 49, 11511 (1994).
15. J.E. Ortega and F.J. Himpsel, Phys. Rev. Lett. **69**, 844-847 (1992); J. E. Ortega, F. J. Himpsel, G. J. Mankey and R. F. Willis, Phys. Rev. B **47**, 1540-1552 (1993).

16. K. Garrison, Y. Chang and P. D. Johnson, Phys. Rev. Lett. 71, 2801 (1993).

17. D. Hartmann, W. Weber, A. Rampe, S. Popovic and G. Güntherodt, Phys. Rev. B **48**, 16837 (1993).

18. P. D. Johnson, K. Garrison, Q. Dong, N. V. Smith, Dongqi Li, J. Mattson, J. Pearson and S. D. Bader, Phys. Rev. B **50**, 8954 (1994).

19. C. Carbone, E. Vescovo, O. Rader, W. Gudat and W. Eberhardt, Phys. Rev. Lett. **71**, 2805 (1993).

20. P. Bruno, J. Magn. Magn. Mater. **121**, 248-252 (1993).

21. N. V. Smith, N. B. Brookes, Y. Chang and P. D. Johnson, Phys. Rev. B **49**, 332 (1994).

22. P. Bruno, J. Appl. Phys. **76**, 6972 (1994).

23. D. D. Koelling, Phys. Rev. B **50**, 273 (1994).

24. J. Mathon, J. Magn. Magn. Mater. **100**, 527 (1991).

25. S.S.P. Parkin, Appl. Phys. Lett. **61**, 1358-1360 (1992).

26. W. Geerts, Y. Suzuki, T. Katayama, K. Tanaka, K. Ando and S. Yoshida, Phys. Rev. B **50**, 12581 (1994).

27. R. Mégy, A. Bounouh, Y. Suzuki, P. Beaunillain, P. Bruno, C. Chappert, B. Lecuyer and P. Veillet, Phys. Rev. B **51**, 5586 (1995).

28. A. Carl and D. Weller, Phys. Rev. Lett. **74**, 190 (1995).

29. P. J. H. Bloemen, M. T. Johnson, M. T. H. van de Vorst, R. Coehoorn, J. J. de Vries, R. Jungblut, J. aan de Stegge, A. Reinders and W. J. M. de Jonge, Phys. Rev. Lett. **72**, 764 (1994).

FIGURES

Fig. 1. Magneto-optical signals for Fe wedges grown at different T_S values. Solid symbols are polar (perpendicular) signals and open circles and curves indicate longitudinal (in-plane) signals. Measurements are at 120, 140, and 110 K, from top to bottom, respectively.)

Fig. 2. T dependence of M_R and of the peak-to-valley difference ΔM_R for two wedges grown at $T_S = 300$ K, showing T_C(surface) and T_N.

Fig. 3. Magnetic phase diagram with respect to growth temperature and Fe thickness. In region I, the films are ferromagnetic with perpendicular easy axes (fct). In region II(a) the films are AF and the surface is ferromagnetic (fcc). In region II(b), the films are ferromagnetic with in-plane easy axes (fct). In region III, the films are ferromagnetic with in-plane easy axes (bcc). (Measurements were performed in the range of 110-190 K.)

Fig. 4 Photoemission spectra ($h\nu$=22.7 eV) of Cu overlayers on 40-Å fcc Co(001). Both the QW states are indicated. Spectra for Cu(001) and 40-Å Co(001) are also shown. Inset: calculated Cu bulk band structure along ΓX (Ref. 19).

Fig. 5. Photoemission spectra of 2-ML Cu overlayer separated from the Cu(001) substrate by a Co wedge. The structure is shown schematically.

Fig. 6. Peak intensities of the *sp*-QW state at 1.6 eV (solid circles) and *d*-QW state at 2.4 eV (open circles; normalized to the same saturation intensities) indicating a more pronounced quantum confinement by the Co barrier for the *d*-QW state. Solid and dashed curves represent the fits described in the text, where t_{Co} is the Co thickness. Inset: Schematic of the minority energy potentials experienced by *sp*- (thick solid line) and *d*- (thick dashed line) electrons, based on the bulk band structures.[20] The energies for the two QW states of 2-ML Cu (thin solid and dashed lines) and their energy differences from the top of the corresponding energy barriers (arrows) are indicated.

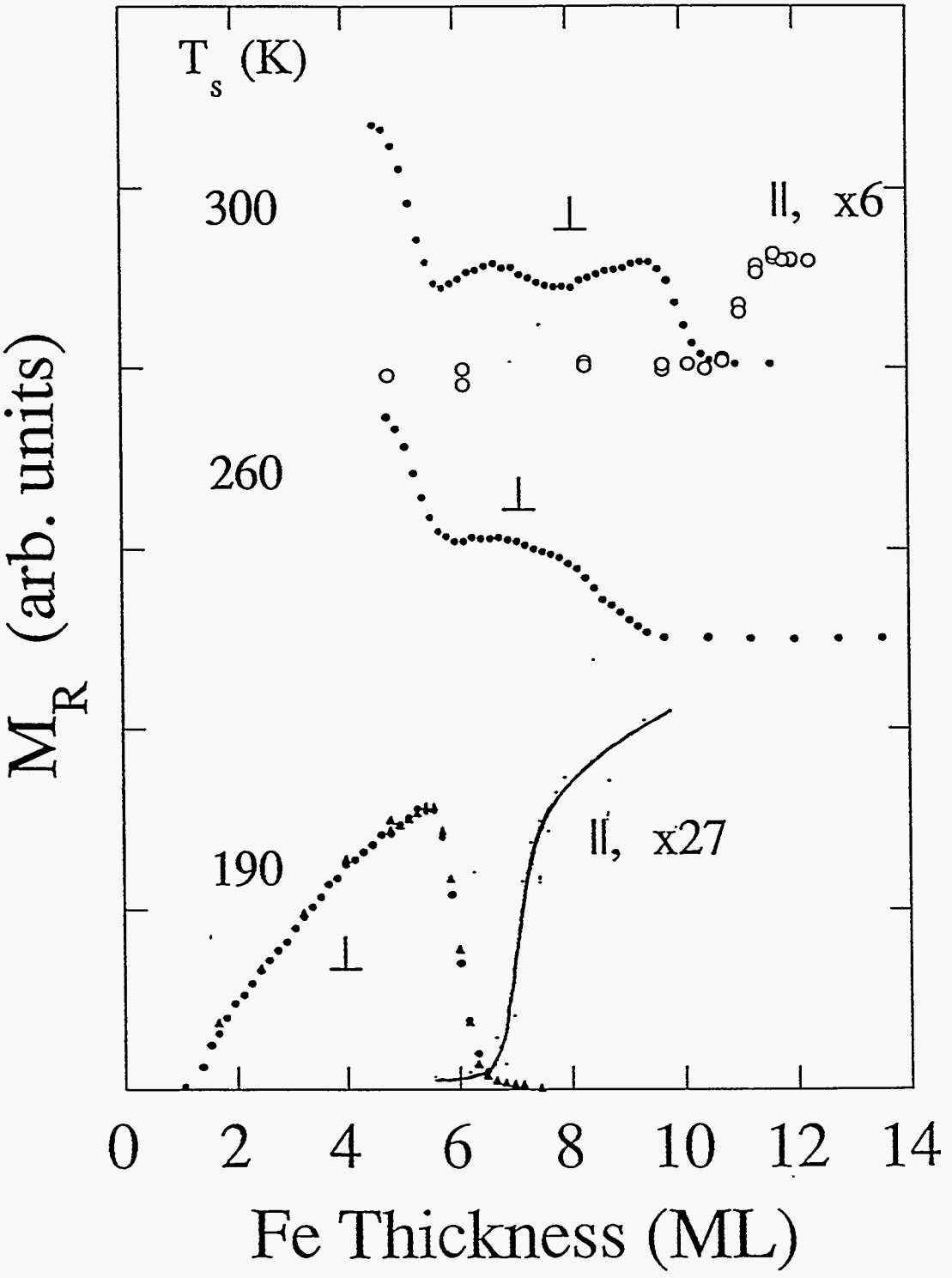
T_s (K)
300
260
190
⊥
∥, x6
∥, x27
M_R (arb. units)
0
2
4
6
8
10
12
14
Fe Thickness (ML)

Fig. 1

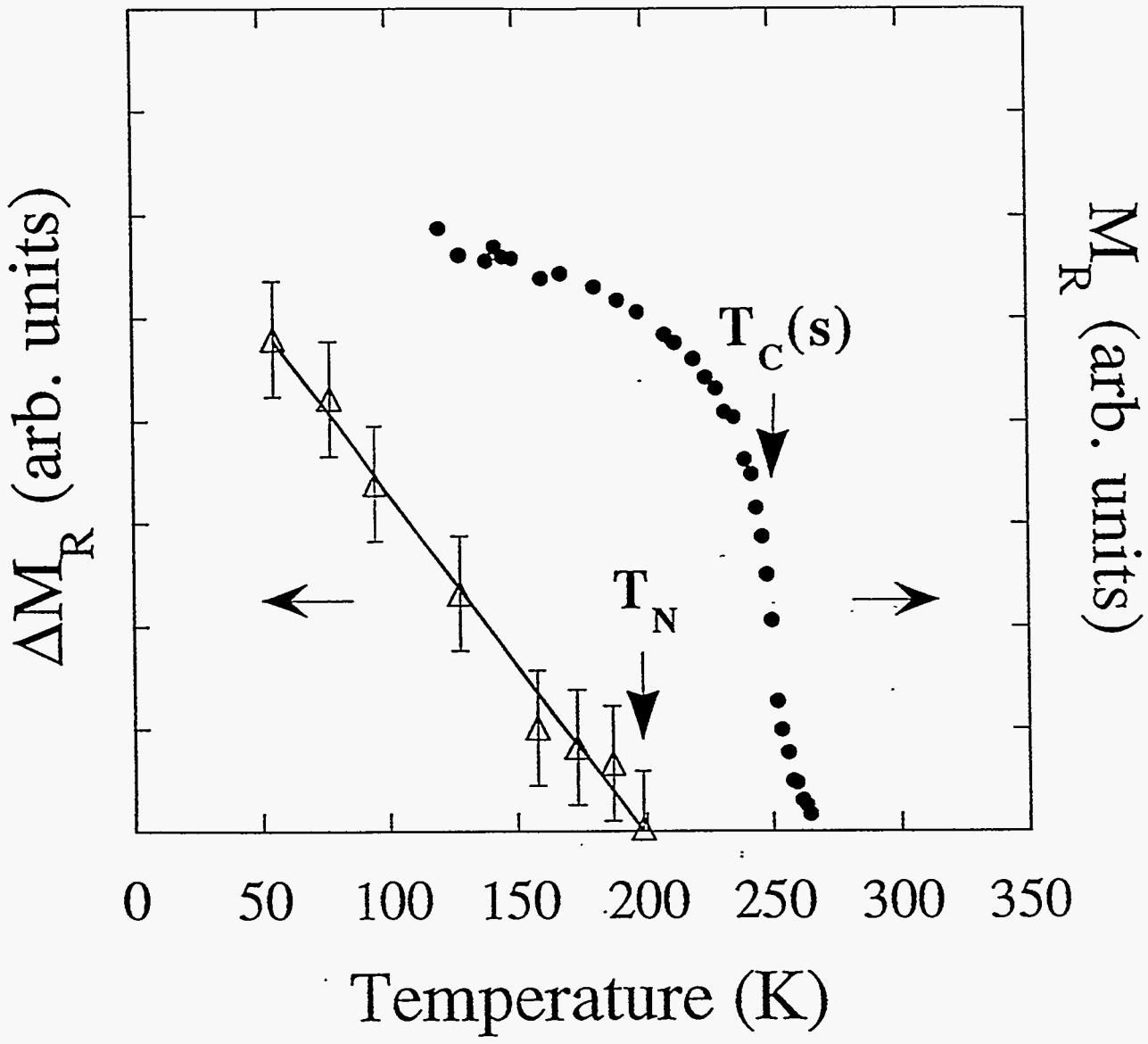
ΔM_R (arb. units)
M_R (arb. units)
T_C(s)
T_N
0
50
100
150
200
250
300
350
Temperature (K)

Fig. 2

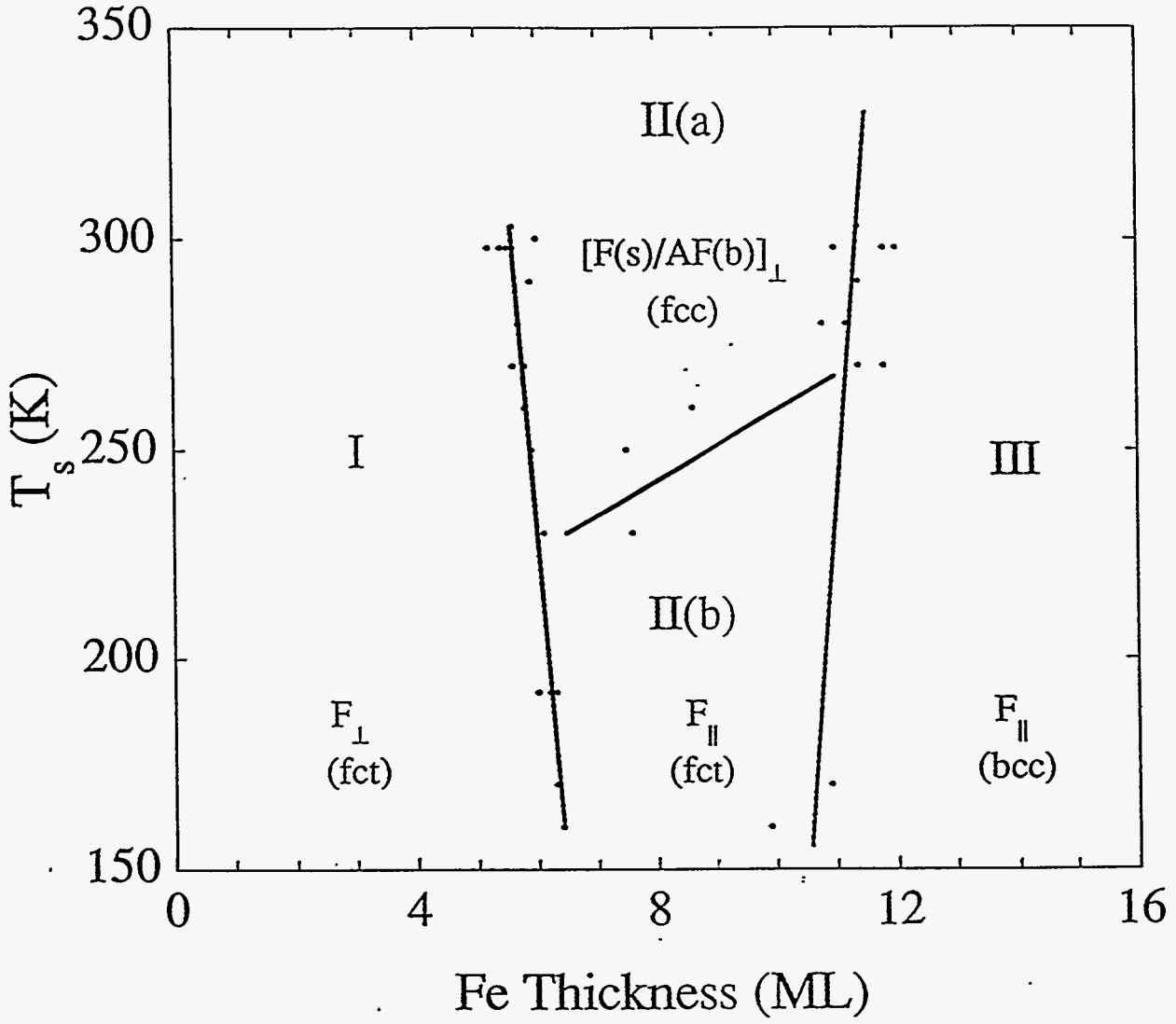
350
300
250
200
150
T_s (K)
0
4
8
12
16
Fe Thickness (ML)
II(a)
$[F(s)/AF(b)]_\perp$
(fcc)
I
III
II(b)
$F_\perp$
(fct)
$F_\parallel$
(fct)
$F_\parallel$
(bcc)

Fig. 3

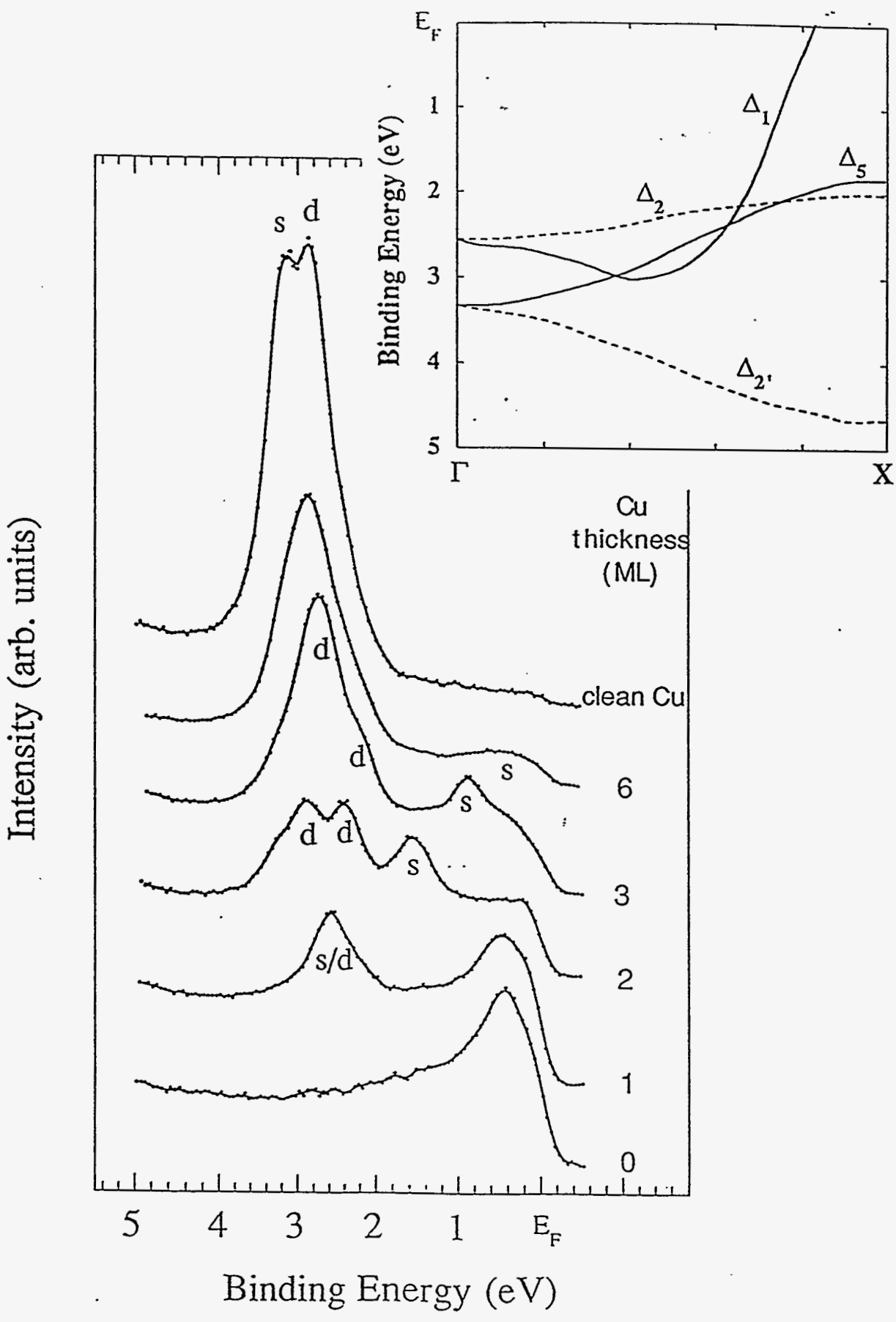
E_F
1
2
3
4
5
Binding Energy (eV)
Δ1
Δ5
Δ2
Δ2'
Γ
X
Cu
thickness
(ML)
clean Cu
6
3
2
1
0
s
d
d
s
d
d
s
s/d
Intensity (arb. units)
5
4
3
2
1
E_F
Binding Energy (eV)

Fig. 4

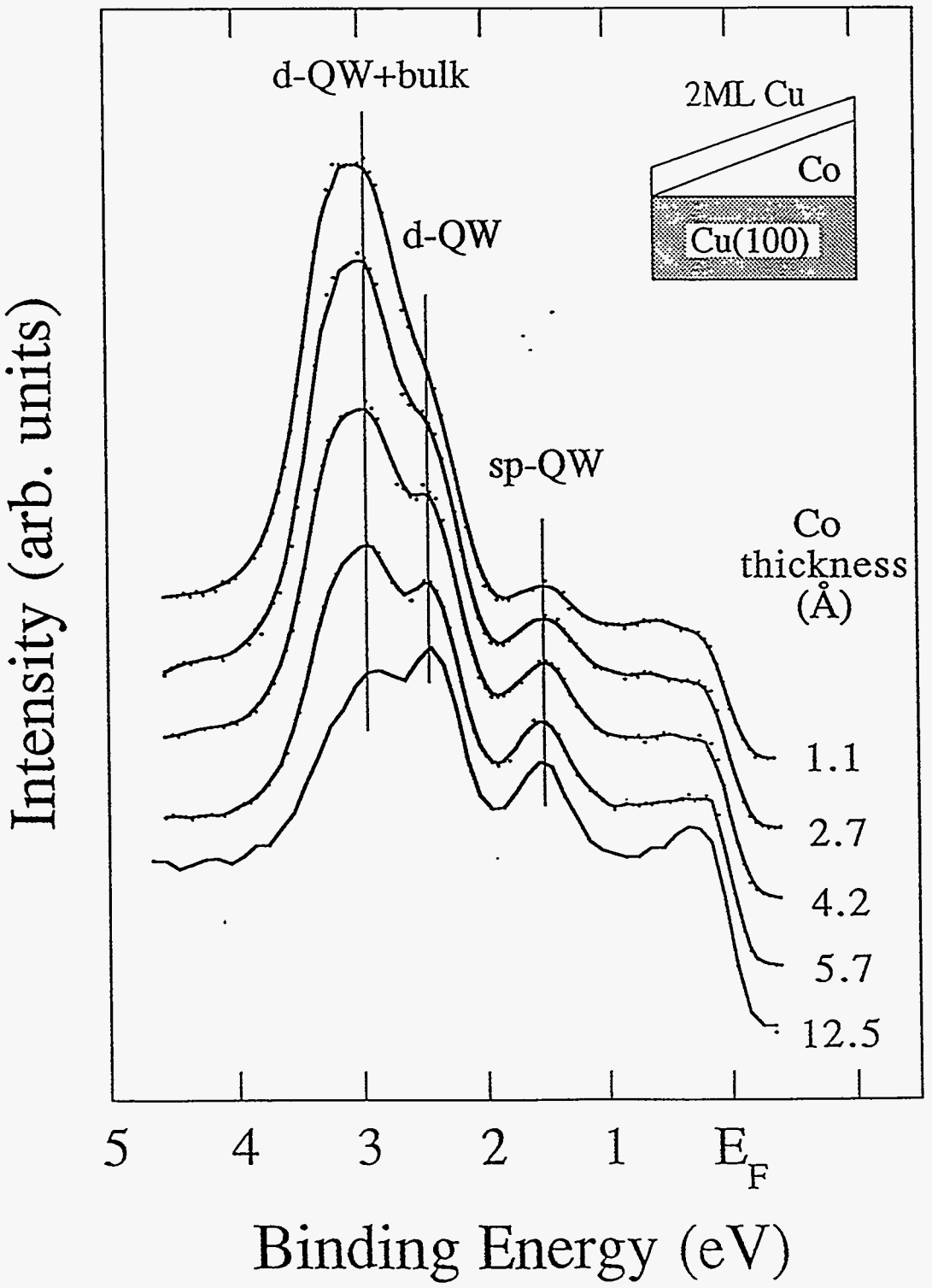
d-QW+bulk
d-QW
sp-QW
2ML Cu
Co
Cu(100)
Co thickness (Å)
1.1
2.7
4.2
5.7
12.5
Intensity (arb. units)
5
4
3
2
1
E_F
Binding Energy (eV)

Fig. 5

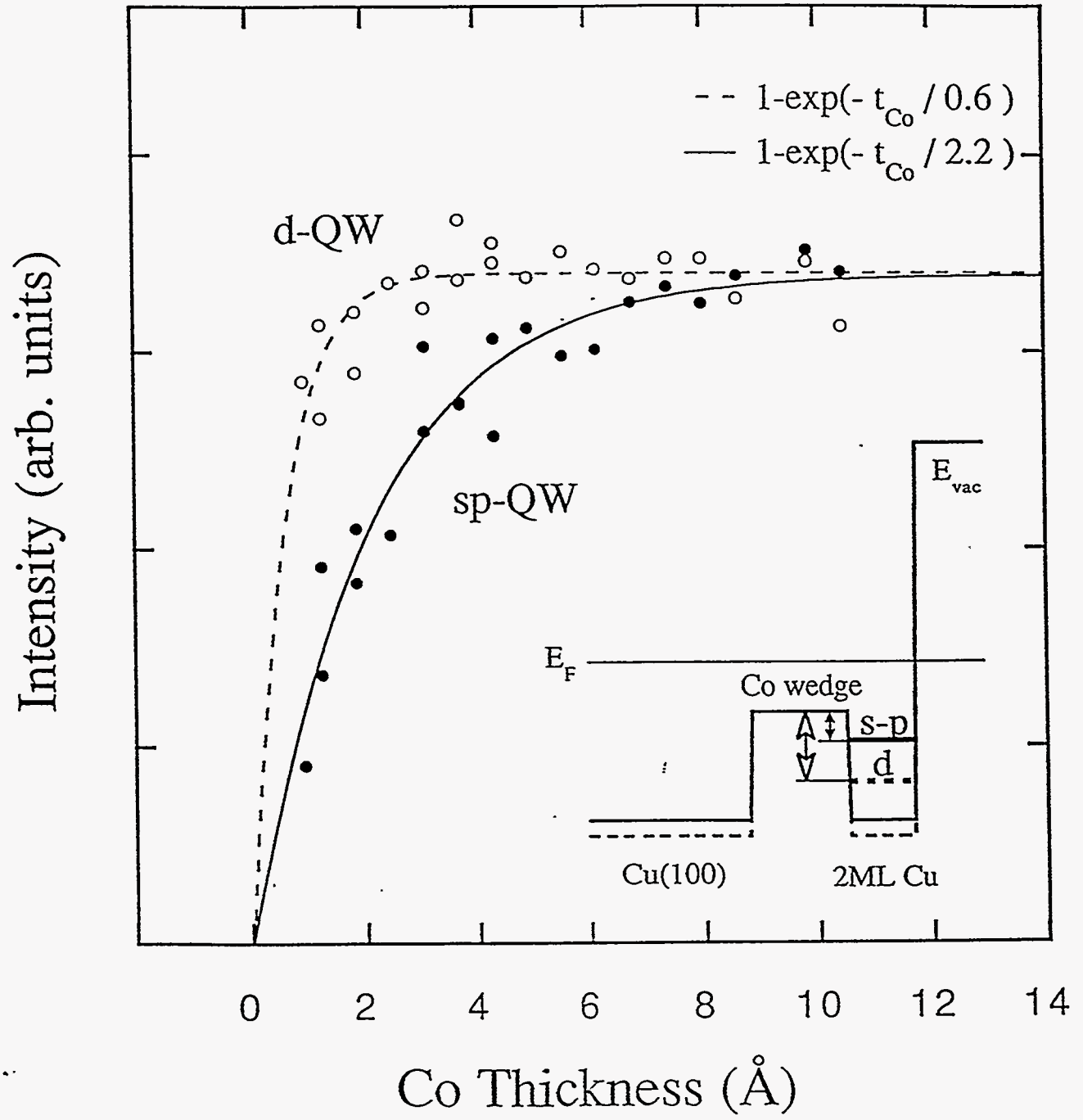
- - 1-exp(- t_Co / 0.6)
—— 1-exp(- t_Co / 2.2)
d-QW
sp-QW
E_vac
E_F
Co wedge
s-p
d
Cu(100)
2ML Cu
Intensity (arb. units)
0
2
4
6
8
10
12
14
Co Thickness (Å)

Fig. 6